Engineering of extracellular vesicles for efficient intracellular delivery of multimodal therapeutics including genome editors

Xiuming Liang (xiuming.liang@ki.se)
Karolinska Institutet
Dhanu Gupta
Karolinska Institutet
Junhua Xie
Ghent University
Elien Wonterghem
Ghent University
Lien Hoecke
Ghent University
Justin Hean
Evox Therapeutics Limited
Zheyu Niu
Shandong First Medical University
Oscar Wiklander
Karolinska Institutet
Wenyi Zheng
Karolinska Institutet
Rim Wiklander
Karolinska Institutet
Rui He
Karolinska Institutet
Doste Mammad
Karolinska Institutet
Jeremy Bost
Scibase Company
Guannan Zhou
Karolinska Institutet
Houze Zhou
Karolinska Institutet
Samantha Roudi

Karolinska Institutet
Antje Zickler
Karolinska Institutet
Andre Gorgens
Karolinska Institutet https://orcid.org/0000-0001-9198-0857
Daniel Hagey
Karolinska Institutet
Olivier G de Jong
Utrecht University
Aileen Uy
Uppsala University
Yuanyuan Zong
Shandong First Medical University
Imre Mager
University of Tartu
Carla Perez
University of Oxford
Thomas Roberts
University of Oxford
Pieter Vader
University Medical Center Utrecht https://orcid.org/0000-0002-7059-8920
Antonin Fougerolles
Evox Therapeutics Limited
Matthew Wood
University of Oxford
Roosmarijn Vandenbroucke
Ghent University
Joel Nordin
Karolinska Institutet
Samir El-Andaloussi
Karolinska Institutet https://orcid.org/0000-0003-4468-9113

Article

Keywords:

Posted Date: October 12th, 2023

DOI: https://doi.org/10.21203/rs.3.rs-3329019/v1

Additional Declarations: Yes there is potential Competing Interest. O.W., J.Z. N., D.G. A.G., M.J.A.W. and S.E.-A. are consultants and stakeholders in Evox Therapeutics Limited, Oxford, United Kingdom. A.D.F., and J.H. are employees of Evox Therapeutics Limited, Oxford, United Kingdom. Other authors declare no conflict of interest. Evox Therapeutics filed a patent application related to the data used in this work. All the data are available in the manuscript or in the supplemental information. Materials are available upon signing the material transfer agreement (MTA) submitted to S.E.-A. and Evox Therapeutics Limited, Oxford, United Kingdom.

Abstract

Intracellular delivery of protein and RNA therapeutics represents a major challenge. Here, we developed highly potent engineered extracellular vesicles (EVs) by incorporating essential bio-inspired attributes required for effective delivery. These comprise engineered mini-intein proteins with self-cleavage activity for active cargo loading and release, and fusogenic VSV-G protein to activate productive endosomal escape. Combining these components allowed high efficiency recombination and genome editing *in vitro*following EV-mediated delivery of Cre recombinase and Cas9/sgRNA RNP cargoes, respectively. *In vivo*, single dose EV-mediated Cre delivery to the brains of Cre-LoxP R26-LSL-tdTomato reporter mice resulted in greater than 40% and 30% recombined cells in hippocampus and cortex respectively. In addition, we demonstrate therapeutic potential of this platform by showing inhibition of LPS-induced systemic inflammation via delivery of a super-repressor of NF-κB activity. Our data establish these engineered EVs as a novel platform for effective delivery of multimodal therapeutic cargoes, including for efficient genome editing.

Full Text

Protein-based therapeutics have unique potential for the treatment of diverse diseases. Whereas there has been great success developing therapeutic proteins against extracellular targets, of which a broad range have been approved for clinical application [1,2], intracellular delivery of proteins remains challenging due to the inherent impermeability of the plasma membrane [3,4]. Thus, numerous strategies have been developed to facilitate intracellular protein delivery. For instance, the iTOP system exploits NaCl-mediated hyperosmolarity and transduction compounds to achieve high efficiency delivery of proteins into primary cells, but this has limited potential for *in vivo* applications [5]. Although Cell-penetrating peptides (CPPs) have also shown promise in some applications, the limitations related to endosomal entrapment and toxicity have been reported [6–8]. Finally, various nanocarriers, such as lipid nanoparticles and polymers, are frequently utilized for intracellular delivery of proteins, but with similar drawbacks to CPPs [9–13].

Another limitation of these strategies is that their synthetic properties induce various side effects when they are applied *in vivo*. Thus, one strategy to overcome these issues is to harness natural delivery vehicles – extracellular vesicles (EVs). EVs are lipid bilayer enclosed particles that are secreted and taken up by all cell types to mediate intercellular trafficking of biologically active molecules [14–16]. However, there are presently two main challenges that must be solved to achieve efficient intracellular delivery of proteins by EVs: i) enrichment of therapeutic proteins inside EVs in a soluble (or non-tethered), active form; and ii) endosomal escape of therapeutic proteins into the cytosol of the target cell.

The enrichment of specific proteins inside of EVs has previously been achieved by fusing the target proteins to the cytoplasmic domain of EV-sorting proteins, such as CD63 [17]. However, as these proteins remain bound to the EV membrane, this approach is not suitable for cytosolic delivery of soluble proteins. To address this limitation, several technologies introducing cleavable linker peptides between the target

protein and EV-sorting domains, and the EXPLORs system have been developed [18,19,20]. Although several of the above technologies have achieved intracellular protein delivery by modifying EVs, these solutions were either dependent on extracellular conditions or required multiple components to be co-expressed. In the present study, we innovatively exploited the engineered self-cleaving mini-intein (intein) derived from *Mycobacterium tuberculosis (Mtu) recA* [21], to connect the EV-sorting protein with the cargo protein, facilitating liberation of soluble cargo protein from the EV-sorting protein inside the EV lumen. This intein comprises the first 110 and last 58 amino acids of the 441 amino acid *Mtu recA* intein, with four additional mutations (C1A, D24G, V67L, and D422G) introduced to enable C-terminal cleavage in a pH-sensitive manner at 37°C [21].

Since endocytosis is the most common mode of biomacromolecular uptake by cells, endosomal entrapment constitutes the primary barrier to the functional intracellular delivery of both therapeutic proteins and EVs [22,23]. Interestingly, fusogenic proteins derived from viruses have been found to mediate endosomal escape and facilitate the release of EV cargo into the cell cytosol [24,25]. In this study, we made use of the fusogenic protein, vesicular stomatitis virus G glycoprotein (VSV-G), as both an efficient endosomal escape activator and EV-sorting protein. Here, we have developed two systems that solve the aforementioned problems above in tandem to achieve high efficiency intracellular protein delivery harnessing engineered EVs (Fig. 1a). Altogether, this work demonstrates the great potential for EV-based therapeutic protein delivery.

Development of the VEDIC system for high efficiency intracellular protein delivery by EVs

Traffic Light (TL) fluorescent Cre reporter cells were exploited to assess the potential of EVs for intracellular delivery of functional proteins (Fig. 1b) [26]. LoxP recombination by Cre results in the excision of the red fluorescent protein (RFP) DsRed which subsequently leads to permanent expression of green fluorescent protein (GFP) (Fig. 1b). EVs derived from Cre alone, CD63-Cre (Cre fused to CD63 to enhance EV-enrichment), CD63-Intein-Cre (self-cleaving protein intein was introduced between CD63 and Cre to liberate Cre from CD63 inside the EV lumen) [21] or Intein-Cre (no EV-sorting domain) overexpressing cells could not achieve any recombination in reporter cells analyzed by flow cytometry (Fig. 1c-e and Supplementary Fig. 1a,c,d). Next, a comprehensive screen of 40 human- and 2 virus-derived fusogenic proteins to identify efficient candidates was performed since fusogenic proteins were reported to enhance EV cargo endosomal escape [27]. While none of the human-derived fusogenic proteins induced Cre-mediated recombination, the fusogenic viral protein VSV-G significantly boosted Cre delivery after co-transfection with CD63-Intein-Cre, such that 66% and 98% of HeLa-TL and T47D-TL cells, respectively, expressed GFP two days after treatment with EVs (Fig. 1f and Supplementary Fig. 1b). Subsequently, we co-expressed VSV-G in the EV producing cells alongside our previously engineered constructs (Fig. 1c) and incubated isolated EVs with reporter cells for 48 hours (h). Of the conditions tested, only VSV-G plus CD63-Intein-Cre EVs achieved significant activity in reporter cells (Fig. 1g), indicating that the EV-sorting

domain (CD63), self-cleaving protein (intein) and endosomal escape booster (VSV-G) were indispensable for the intracellular delivery of Cre by engineered EVs. We term this approach the VEDIC (VSV-G plus EV-Sorting Domain-Intein-Cargo) system.

Next, different doses of the VEDIC EVs were added to reporter cells. We observed a clear pattern of dose-dependent recombination in B16F10-TL, HeLa-TL and T47D-TL cells (Fig. 1h,i, Supplementary Fig. 1e,f and Supplementary Fig. 2a). For VEDIC EVs, a time-lapse video obtained from live imaging of HeLa-TL recipient cells showed increasing recombination over time (Supplementary Video 1), while no GFP signal was observed in the absence of VSV-G (Supplementary Video 2). Furthermore, the protein level of Cre and VSV-G in T47D-TL and B16F10-TL cells was evaluated and showed a correlation with activation of the GFP signal in these cell lines (Fig. 1j and Supplementary Fig. 2c). Moreover, VEDIC EVs were applied to multiple hard-to-transfect cell lines, and we observed significant recombination 2 days after EV addition in all cases (Supplementary Fig. 1g-j and Supplementary Fig. 2b). Finally, CD63 was replaced with other known EV-sorting domains (CD81, CD9 and PTGFRN) and we found that addition of EVs isolated from cells transfected with these additional constructs resulted in significant recombination when combined with VSV-G (Supplementary Fig. 2d).

In addition to adding engineered EVs to reporter cells, the EV-mediated recombination efficiency in co-culture was assessed using direct co-culture (co-culture), IBIDI co-culture µ-slide (IBIDI) and Transwell (Transwell) assays (Supplementary Fig. 3) [29]. For direct co-culture assays, EV-producing and reporter cells were cultured at different ratios and GFP levels were evaluated one day after incubation (Supplementary Fig. 3a). Here, VEDIC expressing cells enabled significant recombination in various reporter cells (Supplementary Fig. 3b-e). For IBIDI co-culture assays, reporter cells were seeded in the inner reservoir as shown in Supplementary Fig. 3f, and the feeder cells were seeded in the 8 surrounding reservoirs. After 4 days of incubation, co-culture with the VEDIC donor cells showed significant levels of GFP activation in the reporter cells (Supplementary Fig. 3g,j). For Transwell assays, the reporter cells were seeded in the lower compartment and the EV-producing cells in the upper chamber (Supplementary Fig. 3f). In line with the previous results, significant increases in the number of GFP positive cells was only observed after co-culture with the VEDIC donor cells, after 4 days of incubation (Supplementary Fig. 3h,i,k).

Development of the VFIC system to further improve intracellular protein delivery by EVs

To further improve the VEDIC system, which requires transfection of several plasmids, we aimed to combine the essential components for intracellular EV cargo delivery into a single construct. To determine whether VSV-G itself could be employed as an efficient EV loading protein, VSV-G-mNG was transfected into HEK293T cells and the isolated vesicles were analyzed by single vesicle flow cytometry after the EVs were stained with a CD63-APC antibody. The total number of mNG + vesicles was far greater than CD63 + vesicles (Fig. 2a). Upon VSV-G-mNG co-transfection with CD63 plasmid in HEK293T cells, the total

number of isolated mNG + vesicles was similar to that of CD63 + vesicles (Fig. 2b). These data imply that VSV-G could function as an EV-sorting domain, similar to CD63. Hence, a VSV-G-Intein-Cre fusion protein was constructed, with and without a foldon component that has been demonstrated to enhance VSV-G trimer formation and function [30,31], and expression of constructs was confirmed (Supplementary Fig. 4d). Upon adding these EVs to reporter cells, a dose-dependent recombination in reporter cells was observed, and nearly 100% recombination in B16F10-TL and T47D-TL cells were detected in the high-dose treated groups (Fig. 2c,d and Supplementary Fig. 4a,b). The VSV-G-Foldon-Intein-Cre (VFIC) performed better than the VSV-G-Intein-Cre construct in low EV-dose experiments (Fig. 2c and Supplementary Fig. 4a), demonstrating the ability of the foldon domain to enhance VSV-G loading and/or function. Time-lapse fluorescence microscopy video analysis revealed similar recombination dynamics using VFIC EVs as was previously observed using the VEDIC system in HeLa-TL cells (Supplementary Video 3). VFIC EV-mediated recombination was also observed in hard-to-transfect cells (Fig. 2e-h and Supplementary Fig. 4c). We subsequently performed the direct co-culture, IBIDI, and Transwell assays using the VFIC system, and got significant recombination in recipient cells by transfer of Cre protein from donor cells (Supplementary Fig. 3k and Supplementary Fig. 4e-h).

The pH-sensitive intein performs C-terminal cleavage during EV-biogenesis

To confirm that the intein we used in this study performed C-terminal cleavage in a pH-dependent manner, we introduced 2 mutants (Fig. 3a). The H439Q variant has a lower pH-sensitivity, which should lead to a lower cleavage rate during EV-biogenesis, since the pH in MVBs is around 6 (Fig. 3a, middle panel) [33]. In contrast, the N440A variant is supposed to abolish the C-terminal cleavage which should lead to minimal cleavage both in EV-producing cells and the isolated EVs (Fig. 3a, lower panel) [34]. As expected, the decrease of C-terminal cleavage to form released Cre cargo protein was corroborated by western blot for the VEDIC system (Fig. 3b). Accordingly, the functional assays (adding isolated EVs to recipient cells or direct co-culture with VEDIC producer cells and reporter cells) showed significantly decreased recombination in reporter cells when the 2 mutants were included in the VEDIC system (Supplementary Fig. 5a-e and Supplementary Fig. 6a). These results were corroborated for the VFIC system (Supplementary Fig. 5f-j and Supplementary Fig. 6b,c). Altogether, these findings support the notion that the intein used for the VEDIC and VFIC technologies enables robust C-terminal cleavage to form soluble cargo proteins in the EV-lumen during EV-biogenesis in a pH-dependent manner (Fig. 1d).

VSV-G boosts endosomal escape following receptor-mediated endocytosis in recipient cells

To ascertain the role of VSV-G in endosomal escape and endocytosis, we introduced mutations that have been described to disrupt fusogenic (P127D) or LDL-R receptor binding capacity (K47Q), respectively (Fig. 3c,d) [35–37]. In order to assess EV uptake and trafficking, Cre was replaced by mNG in the VEDIC

system, which was co-transfected with VSV-G to produce EVs that were added to Huh7 cells [38]. Confocal microscopy was used to evaluate the uptake of the vesicles 48 h after incubation and showed a punctate distribution of green fluorescent signal in recipient cells in the absence of VSV-G, indicating endosomal entrapment (Fig. 3e). However, when VSV-G was included, the mNG signal diffused into the cytosol (Fig. 3e), suggesting endosomal escape. Of note, when P127D was used, mNG instead showed a punctate distribution (Fig. 3f), confirming that endosomal escape was mediated by the fusogenic activity of VSV-G. In line with our hypothesis, mNG was furthermore observed in punctate form when a directly fused CD63-mNG, without intein to liberate cargo protein, was co-transfected with VSV-G (Fig. 3f).

Next, the two mutant VSV-G constructs were used for Cre protein delivery. Decreased Cre protein delivery with the same doses of EVs in HeLa-TL recipient cells was observed using western blot analysis for both mutants compared to the wide-type VSV-G group, given that free Cre protein level was equal in these EV groups (Fig. 3g and Supplementary Fig. 7g) [37]. Utilization of the two VSV-G mutants in the VEDIC system showed significantly decreased Cre-mediated recombination in reporter cells with K47Q and complete loss of reporter activity with P127D after EV treatment, direct co-culture, IBIDI and Transwell assays in different reporter cells (Supplementary Fig. 7a-f). Furthermore, we reproduced these results using the VFIC system (Supplementary Fig. 8).

Robust gene editing by Cas9/sgRNA RNPs and meganuclease targeting PCSK9 using the VEDIC and VFIC systems

Since Cre and mNG proteins were successfully delivered, we next tested whether more relevant therapeutic cargoes could be delivered. To this end, Cre was replaced with Cas9 to encapsulate Cas9-ribonucleoprotein (Cas9-RNP) into engineered EVs (Fig. 4a,b and Supplementary Fig. 9b). As a read-out for Cas9-RNP delivery, we employed CRISPR reporter (Stoplight, SL) cells that constitutively express mCherry followed by a short linker region that includes a sgRNA target region and a stop codon, followed by two eGFP open reading frames (ORFs), +1nt and + 2nt out of frame, respectively. Upon successful Cas9-RNP delivery, non-homology end joining (NHEJ)-mediated + 1nt and + 2nt frameshifts in the targeting linker region will result in bypassing of the stop codon and the permanent expression of eGFP. (Fig. 4c) [39]. Significant dose- and time-dependent genome editing was observed in cells treated with VEDIC and VFIC EVs (Fig. 4d,e and Supplementary Fig. 9a). For VFIC EVs, close to 80% gene editing efficiency was achieved, which is most likely the maximum achievable for this reporter construct (Fig. 4d) [39].

Next, VEDIC and VFIC constructs for the delivery of a previously described meganuclease targeting *PCSK9* were generated (Fig. 4f) [40]. Upon EV exposure to cells, a significant decrease of PCSK9 protein level was observed in a dose-dependent manner (Fig. 4g).

Cre-mediated recombination in melanoma-xenograft and R26-LSL-tdTomato reporter mice by VEDIC and VFIC systems after local injection

Based on the promising results achieved *in vitro*, the *in vivo* applicability of VEDIC and VFIC-engineered EVs was assessed. To evaluate VEDIC and VFIC-mediated Cre delivery *in vivo*, an intratumoral (IT) injection of engineered EVs was conducted in C57BL/6 mice bearing subcutaneous B16F10-TL melanoma xenografts (Supplementary Fig. 10a). 4 days after injection, tumors were harvested for immunohistochemistry analysis, which showed significant GFP signals following treatment with VEDIC and VFIC EVs (Supplementary Fig. 10b). Next, R26-LSL-tdTomato reporter mice, whereby successful Cre delivery excises stop cassettes that are present between the CAG promoter and an ORF of the red fluorescent protein, tdTomato, were exploited for *in vivo* study. These mice were injected with VEDIC and VFIC EVs through intracerebroventricular (ICV) injection for one week to assess Cre delivery in the brain (Fig. 5a) [26]. As shown in Fig. 5b, tdTomato expression was detected in the cerebellum, cortex, and hippocampus of VEDIC- and VFIC EV treated mice. Moreover, we additionally observed trace amounts of tdTomato expression in the olfactory bulb and thalamus of VEDIC and VFIC treated animals (Supplementary Fig. 11a). To further identify which cell types internalized the engineered EVs, the slides were co-stained for both tdTomato and specific cell-marker genes. We found good colocalization of tdTomato with GFAP (astrocyte marker) and IBA1 (microglia marker), but only marginal colocalization of NeuN (neuronal marker) in the corpus callosum and hippocampus in the engineered EV-treated animals (Supplementary Fig. 11b-f). Based on the above results, we concluded that the engineered EVs mainly delivered their cargo to astrocytes and microglia in the brain.

To enhance functional CNS delivery, we next repeated the ICV experiments using osmotic minipumps, allowing for chronic dosing of engineered EVs over 24 h (Fig. 5c). Strikingly, upon flow cytometry analysis of single cells we observed more than 40% and 30% of cells in hippocampus and cortex respectively were edited by Cre delivered via VEDIC system (Fig. 5d). In addition, close to 10% cells in cerebellum were also edited by VEDIC EVs.

Cre recombination in R26-LSL-tdTomato reporter mice following systemic VEDIC and VFIC EV-mediated Cre delivery

Next, one pilot *ex vivo* study was performed by adding engineered EVs to liver primary cells harvested from R26-LSL-tdTomato reporter mice, which showed significant recombination of the cells by VEDIC and VFIC EVs (Supplementary Fig. 12a). Next, engineered EVs were administered via intraperitoneal (IP) injection into R26-LSL-tdTomato reporter mice. The liver, spleen and heart were harvested for analysis by immunofluorescence one week after injection (Fig. 5e). A substantial number of cells in the liver and spleen were found to be tdTomato positive following injection of both VEDIC and VFIC EVs, but not after injection of CD63-Intein-Cre EVs (Fig. 5f). In contrast, we did not observe any significant tdTomato expression in the EV hard-to-reach organ, heart (Supplementary Fig. 13b).

After co-staining of tdTomato together with cell specific markers, a high degree of functional delivery to leukocyte (CD45), especially to the T cell population (CD3) and macrophages (F4/80), was detected

(Fig. 6g,i and Supplementary Fig. 12c,d,e,g). In contrast, B cells (B220) showed low recombination events *in vivo* (Fig. 5h and Supplementary Fig. 12f).

Treatment of Lipopolysacharide (LPS)-induced systemic inflammation by VEDIC and VFIC-mediated delivery of super-repressor of NF-κB

To demonstrate the applicability of our systems for the treatment of disease, we applied the VEDIC and VFIC EVs to treat lipopolysaccharide (LPS)-induced systemic inflammation by delivering a previously reported super-repressor of NF-κB activity (SR) (Supplementary Fig. 13a) [41]. To accomplish this, CD63-Intein-SR, VSV-G-Intein-SR and VSV-G-Foldon-Intein-SR constructs were generated, and HEK-Blue-NF-κB luciferase reporter cells were used as a read-out for functional *in vitro* assessment of the system (Fig. 6a,b and Supplementary Fig. 13d). In this reporter cell line, IκB is degraded upon inflammatory stimuli such as LPS or TNF-α stimulation, which allows NF-κB to translocate to the nucleus and drive downstream luciferase reporter gene expression, since luciferase is driven by a minimal NF-κB promoter (Fig. 6c) [42]. First, we confirmed that the NF-κB SR, which is constitutionally active and maintains the NF-κB in the cytoplasm, inhibited the HEK-Blue-NF-κB luciferase reporter activation (Supplementary Fig. 13b,c) [43]. SR delivered by VSV-G-Foldon-Intein-SR, VSV-G-Intein-SR, and VSV-G + CD63-Intein-SR EVs successfully inhibited TNF-α-mediated NF-κB signaling activation evidenced by decreased reporter gene expression (Fig. 6d,e). This provided the rationale for testing these EVs in a murine LPS-induced model of systemic inflammation (Fig. 6f). Thus, engineered EVs were injected 4 h before and 6 h after injecting LPS to allow for, and enhance, the binding of EV-delivered SR to NF-κB, respectively. Subsequently, the weight and mortality of the mice were measured at 24 and 48 h after LPS treatment respectively. Compared to the PBS and CD63-Intein-SR injected groups, the body weight and survival of VSV-G + CD63-Intein-SR and VSV-G-Foldon-Intein-SR treated animals was significantly improved after 48 h (Fig. 6g,h). Histology of the liver revealed a decrease of inflammatory cells at the portal areas as well as a significant alleviation of the hydropic degeneration of hepatocytes by treatment with both VEDIC and VFIC engineered EVs (Fig. 6i). These results demonstrate the adaptability and therapeutic potential of the VEDIC and VFIC systems for the treatment of disease.

Conclusions

By fine-tuning our engineering strategies, we have identified solutions to the major bottlenecks, the enrichment of free-form active cargo into EVs and their endosomal escape in recipient cells, to EV-mediated intracellular protein delivery. The resulting VEDIC and VFIC systems achieved an unprecedented level of efficiency for EV-mediated intracellular delivery of functional proteins *in vitro* and *in vivo*. Owing to the versatility of the VEDIC and VFIC systems, we anticipate that many other therapeutic proteins or protein complexes of interest could be efficiently delivered, apart from Cre, super-repressor of NF-κB and Cas9-RNPs explored in this work. As such, these approaches may hold great potential for the further therapeutic development.

Importantly, more than 40% and 30% cells in hippocampus and cortex respectively were edited by Cre delivered via VEDIC system after osmotic pump ICV injection, the efficiency of which is even comparable to the traditional AAV-mediated protein delivery [44,45]. Encouraged by this, we anticipate the development of therapeutics for central nervous system (CNS) genetic diseases, such as Huntington's disease and spinal muscular atrophy [46,47], through delivery of gene editing tools (CRISPR/Cas9 or base editors) to the brain using engineered EVs.

Furthermore, we applied engineered EVs for the treatment of LPS-induced systemic inflammation, demonstrating that therapeutic levels of intracellular protein delivery were achieved by our systems *in vivo*. These observations demonstrate the therapeutic potential of these approaches, which shows exciting promise for the potential development of treatments for a wide array of pathologies, such as lysosomal storage diseases (LSDs) and enzymatic deficiencies [48,49]. To summarize, the VEDIC and VFIC systems developed in this study allow for robust intracellular functional delivery of therapeutic proteins, both *in vitro* and *in vivo*. In addition, the high genome editing efficiency achieved by Cas9-RNP delivery implies that this strategy may lead to potential applications in the treatment of genetic diseases.

Declarations

Acknowledgements

We apologize to the researchers whose work is closely related to this study but cannot be cited because of limited space. The confocal imaging was performed at the Live Cell Imaging unit/Nikon Center of Excellence, BioNut, Karolinska Institutet. This study was supported by H2020 (EXPERT), the Swedish foundation of Strategic Research (FormulaEx, SM19-0007), ERC CoG (DELIVER) and the Swedish Research Council (4–258/2021) got by S.E.-A.; by the Swedish Research Council (VR), Grant for half-time research position in a clinical environment (2021-02407), and the CIMED junior investigator grant got by J.Z.N.; by the Swedish Research Council (VR), Grant for half-time research position in a clinical environment (2022-02449), and the CIMED junior investigator grant (FoUI-976434) got by O.W.; and by Evox Therapeutics Limited.

Author contributions

Conceptualization: X.L., D.G., J.H., I.M., J.Z.N and S.E.-A. Methodology: X.L., J.X., Z.N., E.V.W., L.V.H., O.W., W.Z., R.J.W., R.H., D.R.M., J.B., G.Z., H.Z., S.R., A.Z., A.G., D.W.H., O.G.J., A.G.U., Y.Z., C.M.P., T.C.R., and R.E.V. Investigation: X.L., D.G., J.X., Z.N., E.V.W., L.V.H., O.W., W.Z., R.J.W., R.H., D.R.M., J.B., G.Z., H.Z., S.R., A.Z., A.G., D.W.H., O.G.J., A.G.U., Y.Z., C.M.P., T.C.R., Z.J.N., R.E.V., and S.E.-A. Visualization: X.L., D.G., J.X., Z.J.N., R.E.V., and S.E.-A. Funding acquisition: Z.J.N., O.W., and S.E.-A. Supervision: S.E.-A. Writing: X.L. Editing: X.L., D.H., O.G.J., T.C.R., Z.J.N., O.W., D.G., A.G.U., A.D.F., M.J.A.W., and S.E.-A.

Competing interests

O.W., J.Z. N., D.G. A.G., M.J.A.W. and S.E.-A. are consultants and stakeholders in Evox Therapeutics Limited, Oxford, United Kingdom. A.D.F., and J.H. are employees of Evox Therapeutics Limited, Oxford, United Kingdom. Other authors declare no conflict of interest. Evox Therapeutics filed a patent application related to the data used in this work. All the data are available in the manuscript or in the supplemental information. Materials are available upon signing the material transfer agreement (MTA) submitted to S.E.-A. and Evox Therapeutics Limited, Oxford, United Kingdom.

Ethics: The animal work of this study was approved by Karolinska University hospital and the authors got all the related ethical permits.

References

1. Messersmith, W. A. & Ahnen, D. J. Targeting EGFR in Colorectal Cancer. *N. Engl. J. Med.* **359**, 1834–1836 (2022).

2. Reck, M. *et al.* Safety and patient-reported outcomes of atezolizumab plus chemotherapy with or without bevacizumab versus bevacizumab plus chemotherapy in non-small-cell lung cancer. *Journal of Clinical Oncology* **38**, 2530–2542 (2020).

3. Stewart, M. P. *et al.* In vitro and ex vivo strategies for intracellular delivery. *Nature* **538**, 183–192 (2016).

4. Goswami, R., Jeon, T., Nagaraj, H., Zhai, S. & Rotello, V. M. Accessing Intracellular Targets through Nanocarrier-Mediated Cytosolic Protein Delivery. *Trends Pharmacol Sci* **41**, 743–754 (2020).

5. D'Astolfo, D. S. *et al.* Efficient intracellular delivery of native proteins. *Cell* **161**, 674–690 (2015).

6. Fu, J., Yu, C., Li, L. & Yao, S. Q. Intracellular Delivery of Functional Proteins and Native Drugs by Cell-Penetrating Poly(disulfide)s. *J Am Chem Soc* **137**, 12153–12160 (2015).

7. Steinauer, A. *et al.* HOPS-dependent endosomal fusion required for efficient cytosolic delivery of therapeutic peptides and small proteins. *Proc Natl Acad Sci U S A* **116**, 512–521 (2019).

8. Wadia, J. S., Stan, R. V. & Dowdy, S. F. Transducible TAT-HA fusogenic peptide enhances escape of TAT-fusion proteins after lipid raft macropinocytosis. *Nat Med* **10**, 310–315 (2004).

9. Boehnke, N. *et al.* Massively parallel pooled screening reveals genomic determinants of nanoparticle delivery. *Science (1979)* **377**, (2022).

10. Chakravarty, P., Qian, W., El-Sayed, M. A. & Prausnitz, M. R. Delivery of molecules into cells using carbon nanoparticles activated by femtosecond laser pulses. *Nat Nanotechnol* **5**, 607–611 (2010).

11. Liu, B., Ianosi-Irimie, M. & Thayumanavan, S. Reversible Click Chemistry for Ultrafast and Quantitative Formation of Protein-Polymer Nanoassembly and Intracellular Protein Delivery. *ACS Nano*

13, 9408–9420 (2019).

12. Yan, M. *et al.* A novel intracellular protein delivery platform based on single-protein nanocapsules. *Nat Nanotechnol* **5**, 48–53 (2010).

13. Zuris, J. A. *et al.* Cationic lipid-mediated delivery of proteins enables efficient protein-based genome editing in vitro and in vivo. *Nat Biotechnol* **33**, 73–80 (2015).

14. Kamerkar, S. *et al.* Exosomes facilitate therapeutic targeting of oncogenic KRAS in pancreatic cancer. *Nature* **546**, 498–503 (2017).

15. Herrmann, I. K., Wood, M. J. A. & Fuhrmann, G. Extracellular vesicles as a next-generation drug delivery platform. *Nat Nanotechnol* **16**, 748–759 (2021).

16. Mehanny, M., Lehr, C. M. & Fuhrmann, G. Extracellular vesicles as antigen carriers for novel vaccination avenues. *Adv Drug Deliv Rev* **173**, 164–180 (2021).

17. Liang, X. *et al.* Extracellular vesicles engineered to bind albumin demonstrate extended circulation time and lymph node accumulation in mouse models. *J Extracell Vesicles* **11**, (2022).

18. Banskota, S. *et al.* Engineered virus-like particles for efficient in vivo delivery of therapeutic proteins. *Cell* **185**, 250-265.e16 (2022).

19. Somiya, M. & Kuroda, S. Reporter gene assay for membrane fusion of extracellular vesicles. *J Extracell Vesicles* **10**, (2021).

20. Yim, N. *et al.* Exosome engineering for efficient intracellular delivery of soluble proteins using optically reversible protein-protein interaction module. *Nat Commun* **7**, 1–9 (2016).

21. Wood, D. W., Wu, W., Belfort, G., Derbyshire, V. & Belfort, M. A genetic system yields self-cleaving inteins for bioseparations. *Nat Biotechnol* **17**, 889–892 (1999).

22. Mulcahy, L. A., Pink, R. C. & Carter, D. R. F. Routes and mechanisms of extracellular vesicle uptake. *J Extracell Vesicles* **3**, 1–14 (2014).

23. Gilleron, J. *et al.* Image-based analysis of lipid nanoparticle-mediated siRNA delivery, intracellular trafficking and endosomal escape. *Nat Biotechnol* **31**, 638–646 (2013).

24. Zhang, X. *et al.* Programmable Extracellular Vesicles for Macromolecule Delivery and Genome Modifications. *Dev Cell* **55**, 784-801.e9 (2020).

25. Albanese, M. *et al. MicroRNAs are minor constituents of extracellular vesicles that are rarely delivered to target cells*. *PLoS Genetics* vol. 17 (2021).

26. Zomer, A., Steenbeek, S. C., Maynard, C. & Van Rheenen, J. Studying extracellular vesicle transfer by a Cre-loxP method. *Nat Protoc* **11**, 87–101 (2016).

27. Mangeot, P. E. *et al.* Protein transfer into human cells by vsv-g-induced nanovesicles. *Molecular Therapy* **19**, 1656–1666 (2011).

28. Görgens, A. *et al.* Optimisation of imaging flow cytometry for the analysis of single extracellular vesicles by using fluorescence-tagged vesicles as biological reference material. *J Extracell Vesicles* **00**, (2019).

29. Zomer, A. *et al.* In vivo imaging reveals extracellular vesicle-mediated phenocopying of metastatic behavior. *Cell* **161**, 1046–1057 (2015).

30. Vogel, A. B. *et al.* BNT162b vaccines protect rhesus macaques from SARS-CoV-2. *Nature* **592**, 283–289 (2021).

31. Papanikolopoulou, K., Forge, V., Goeltz, P. & Mitraki, A. Formation of Highly Stable Chimeric Trimers by Fusion of an Adenovirus Fiber Shaft Fragment with the Foldon Domain of Bacteriophage T4 Fibritin. *Journal of Biological Chemistry* **279**, 8991–8998 (2004).

32. Callanan, J. *et al.* Expansion of known ssRNA phage genomes: From tens to over a thousand. *Sci Adv* **6**, (2020).

33. Chong, S. *et al.* Utilizing the C-terminal cleavage activity of a protein splicing element to purify recombinant proteins in a single chromatographic step. **26**, 5109–5115 (1998).

34. Roey, P. Van *et al.* Crystallographic and Mutational Studies of Mycobacterium tuberculosis recA Mini-inteins Suggest a Pivotal Role for a Highly Conserved Aspartate Residue. *J Mol Bio.* **1**, 162–173 (2007).

35. Votteler, J. *et al.* Designed proteins induce the formation of nanocage-containing extracellular vesicles. *Nature* **540**, 292–295 (2016).

36. Fredericksen, B. L. & Whitt, M. A. Vesicular stomatitis virus glycoprotein mutations that affect membrane fusion activity and abolish virus infectivity. *J Virol* **69**, 1435–1443 (1995).

37. Nikolic, J. *et al.* Structural basis for the recognition of LDL-receptor family members by VSV glycoprotein. *Nat Commun* **9**, 1–12 (2018).

38. Wan, T. *et al.* Exosome-mediated delivery of Cas9 ribonucleoprotein complexes for tissue-specific gene therapy of liver diseases. *Sci Adv.* **2017**, 1–14 (2022).

39. de Jong, O. G. *et al.* A CRISPR-Cas9-based reporter system for single-cell detection of extracellular vesicle-mediated functional transfer of RNA. *Nat Commun* **11**, 1–13 (2020).

40. Wang, L. *et al.* Meganuclease targeting of PCSK9 in macaque liver leads to stable reduction in serum cholesterol. *Nat Biotechnol* **36**, 717–725 (2018).

41. Schreiber, J., Efron, P. A., Park, J. E., Moldawer, L. L. & Barbul, A. Adenoviral gene transfer of an NF-κB super-repressor increases collagen deposition in rodent cutaneous wound healing. *Surgery* **138**, 940–946 (2005).

42. Liu, T., Zhang, L., Joo, D. & Sun, S. C. NF-κB signaling in inflammation. *Signal Transduct Target Ther* **2**, (2017).

43. Kim, S. *et al.* Exosome-based delivery of super-repressor IκBα ameliorates kidney ischemia-reperfusion injury. *Kidney Int* **100**, 570–584 (2021).

44. Lang, J. F., Toulmin, S. A., Brida, K. L., Eisenlohr, L. C. & Davidson, B. L. Standard screening methods underreport. *Nat Commun* 1–10 doi:10.1038/s41467-019-11321-7.

45. Kaspar, B. K. *et al.* Adeno-associated virus effectively mediates conditional gene modification in the brain. *Proc. Natl. Acad. Sci. U. S. A.* **99**, 2320-2325 (2002).

46. Tu, Z. *et al.* Cas9-mediated replacement of expanded CAG repeats in a pig model of Huntington ' s disease. *Nat. Biomed. Eng.* **7,** 629-646 (2023).

47. To, L. & Editor, T. H. E. Base editing-mediated splicing correction therapy for spinal muscular atrophy. *Cell Res.* **30**, 548-550 (2020).

48. Platt, F. M., d'Azzo, A., Davidson, B. L., Neufeld, E. F. & Tifft, C. J. Lysosomal storage diseases. *Nat Rev Dis Primers* **4**, (2018).

49. Burton, B. K., Kar, S. & Kirkpatrick, P. Sapropterin. *Nat Rev Drug Discov* **7**, 199–200 (2008).

Methods

Materials: see the Supplementary Table 1 key reagents resources.

Cell lines

HEK293T cells used to produce the functional EVs in this study were maintained in Dulbecco's Modified Eagle Medium (DMEM) (high glucose) supplemented with 10% fetal bovine serum (FBS) (Gibco, USA) and 1% Antibiotic-Antimycotic (Anti-anti) (Gibco, USA). Cells were cultured at 37°C in a humidified air atmosphere containing 5% CO_2. The reporter cell lines (Hela-TL, T47D-TL, B16F10-TL, Raw264.7-TL, HEK-Blue-NF-κB and HEK293T-SL) were cultured using the same medium and the same conditions as HEK293T cells. THP-1-TL, K562-TL and MSC-TL cells were cultivated in Roswell Park Memorial Institute (RPMI) 1640 medium (high glucose) supplemented with 10% FBS and 1% Anti-anti.

Mice model (Intra-tumor injection)

C57BL/6 mice (5 weeks of age, 20 g body weight) were acclimated to their new surroundings at least one week before the experiment. B16F10-TL cells resuspended in PBS were inoculated subcutaneously into the mice at a density of 0.5 million cells per mouse. Ten days after inoculation when obvious tumors were formed, engineered EVs were injected directly into the tumors. The injected volume was 50 µL per mouse with 7.5×10^{10} EVs. Four days after intra-tumor injection of EVs, the mice were sacrificed, and tumors were harvested and fixed in PFA. Tumor tissues were stained immunohistochemically for GFP expression while tissues in lysis buffer were homogenised using a tissue lyser machine.

Mice model (LPS-induced inflammation)

C57BL/6 mice (5 weeks of age, 20 g body weight) were acclimated to their new surroundings at least one week before the experiment. Animals were injected (IP) with engineered EVs 4 h before IP injection of LPS (Sigma, USA) at the dose of 7.5 mg/Kg. Six hours after LPS induction, engineered EVs were IP injected once more to boost the intracellular delivery of the protein cargos by EVs. The survival rate and body weight of the mice with LPS induction were recorded for 2 days. 48 hours after LPS induction, the mice were euthanized and sacrificed, and main organs, such as liver, were harvested and fixed with PFA. H&E (haematoxylin and eosin) staining was performed to check the extent of damage to the organs induced by LPS. The damage of the tissues was evaluated by a professional pathologist.

Mice model (ICV delivery of EVs via osmotic pump)

For a constant intracerebroventricular delivery of the EV preparations, Alzet® osmotic pumps (2001D) were used. These pumps were filled with 200 µl of the EV preparation at a concentration of $4x10^{12}$ EVs/ml. The osmotic pumps were prepared and implanted as described by Sanchez-Mendoza and colleagues. In short, 15 weeks old R26-LSL-tdTomato reporter mice (B6.Cg-*Gt(ROSA)26Sor*$^{tm9(CAG\text{-}tdTomato)Hze}$/J (*Rosa26.tdTomato*)) reporter mice were anesthetized with isoflurane and mounted on a stereotactic frame. A constant body temperature of 37 °C was maintained using a heating pad. Next, a small incision in the skin was made from the base of the neck to up in between the eyes. The injection needle of the pump system was placed in the ventricles based on coordinates measured relative to the bregma intersection (anteroposterior 0.07 cm, mediolateral 0.1 cm, dorsoventral 0.2 cm). The cannula was fixed to the skull with Loctite 454. A subcutaneous pocket for the osmotic pump was made by using a blunted scissor to slide underneath the skin at the base of the neck. Next the pumps were inserted under the skin at the base of the neck and pushed to the back as far as was possible without resistance. The osmotic pump was connected to the cannula via a vinyl catheter (0.71 mm outer diameter). An immediate constant delivery of the EV preparations started upon implantation of the pumps at a flow rate of 8 µl/hour. After surgery the incision was sutured and 48hours after the implantation, the pumps were removed, and bone wax was used to close the skull again.

Construct generation

All the transgenes, except the ones purchased from Addgene and the human-derived fusogens, were ordered from IDT (Integrated DNA Technologies, USA). The transgenes were first cloned into the pLEX vector backbone using EcoRI and XhoI sites. The constructs used in this study were then generated from the ordered fragments through restriction enzyme digestion and subsequent self-ligation. VSV-G-Intein-Cre and VSVG-Foldon-Cre were generated from the VSV-G-Foldon-Intein-Cre construct using Kpn2I and MluI, respectively. For VSV-G-Cre, VSV-G-Intein-Cre was digested with MluI. CD63-Intein-RS was generated by digesting VSV-G-Foldon-Intein-RS and CD63-Intein-Cre with BamHI and XhoI, and then inserting RS into the resulting CD63-Intein vector. Similarly, to synthesize CD63-Intein-Cas9 and VSV-G-Foldon-Intein-Cas9 constructs, CD63-Intein-Cre and VSV-G-Foldon-Intein-Cre were digested with BamHI and XhoI, and Cas9 inserted into CD63-Intein and VSV-G-Foldon-Intein, respectively. The CD63-Intein-M1 and VSV-G-Foldon-Intein-M1 constructs were generated by replacing Cre with M1 (M1 PCSK9 meganuclease) using BamHI and XhoI digestion. The 40 human-derived fusogens were ordered from Twist (Twist Bioscience) and the vector used was pTwist CMV BetaGlobin.

Plasmid transfection

HEK293T cells were seeded into 15-cm dishes, with the numbers of dishes decided according to the amount of EVs to be used in indicated experiments. Polyethylenimine (PEI, Polysciences) was utilized for the transfection of plasmid/s according to the protocol provided by the manufacturer. The ratio of PEI to plasmid was 2:1 in this study. For single plasmid transfection, 30 µg plasmid was used for each plate. For co-transfection of 2 plasmids, 20 µg of each plasmid was used while for 3 plasmids, 15 µg of each plasmid was used.

EV production

EVs were produced by transient transfection of the transgenes using polyethylenimine. HEK293T cells were seeded into 15-cm dishes at a density of 5 million cells per dish using complete DMEM medium. After 2 days, the cells were transfected with the transgenes and the medium changed to Opti-MEM (Gibco, USA) with 1% Anti-anti 6 h post-transfection. After 48 h, the conditioned medium (CM) was collected and centrifuged (700 x g for 5 min followed by 2,000 x g for 10 min). The supernatant was then filtered through a 0.22 µm filter system.

EV isolation

Tangential flow filtration (TFF, MicroKross, 20 cm^2, Spectrum labs) was used to isolate EVs from the filtered CM. Particles greater than the 300 kDa cutoff of the TFF were retained in the system and concentrated. These particles were further concentrated using Amicon Ultra-15 100 kDa (Millipore) spin filters, which were centrifuged at 4,000 x g for 30 min to several hours at 4°C, depending on the amount EVs in the samples. Lastly, the concentrated EVs were collected in maxirecovery 1.5 ml Eppendorf tubes (Axygene, USA) and quantified using Nanoparticle Tracking Analysis (NTA).

Nanoparticle Tracking Analysis (NTA)

EV samples were diluted with freshly 0.22 μm-filtered PBS before checking the particle sizes and concentrations using the NanoSight NS500 instrument. Five videos of more than 30 second durations each were taken at the camera level of 15 in light scatter mode. All the samples were analysed with the same setting using the NTA 2.3 software.

Traditional flow cytometry

After the different traffic-light reporter cells were added into EVs at different time points, or after the reporter cells were co-cultured with EV-producing cells for 24 h, GFP expression was quantified using the MACSQuant Analyzer 10 flow cytometer (Miltenyi Biotec, Germany). Briefly, the cells in 96-well plates were washed with PBS once and trypsinized for 5 min at 37°C. The trypsin was then neutralized using cell medium supplemented with 10% FBS. After adding DAPI to check the cell viability, the cells were sampled by the MACSQuant analyzer using the settings of one specific reporter cell line for all the measurements. The FlowJo software (version 10.6.2) was used to calculate the percentage of GFP positive cells.

Single-vesicle flow cytometry

HEK293T cells were either transfected with VSV-G-mNeonGreen construct only or co-transfected with VSV-G-mNeonGreen and CD63. Six hours post-transfection, the medium was changed to Opti-MEM medium (Gibco, USA) with 1% Anti-anti. After 2 days, the medium was harvested and centrifuged at 700 x g for 5 min, followed by 2,000 x g for 10 min and subsequently filtered through a 0.22 μm filter system. In a v-bottom 96-well plate, 25 μl of each sample was incubated with APC-labelled CD63 antibody (Miltenyi Biotec, Germany; 1 nM per well) overnight under dark conditions. The samples were then diluted 1000 times and transferred into an R-bottom 96-well plate. Amnis® CellStream instrument (Luminex, US) was utilized to evaluate the engineered EVs at single-vesicle level. The collected data was then analysed using FlowJo software (version 10.6.2).

EV-addition assays in reporter cells

The reporter cells used in this study were seeded into 96-well plates at the following densities: 1×10^4 (Hela-TL), 2×10^4 (T47D-TL), 1.5×10^4 (B16F10-TL), 5×10^4 (Raw264.7-TL), 5×10^4 (THP-1-TL), 5×10^4 (K562-TL), 1×10^4 (MSC-TL), 8×10^3 (HEK-SL) and 2×10^4 (HEK-Blue-NF-κB) cells per well. The following day, different doses of EVs were added directly into each of the reporter cells, except for HEK-Blue-NF-κB. The doses of the EVs used and the time for incubation are indicated in each Fig.. GFP positive cells were confirmed either by fluorescent microscopy or by MACSQuant flow cytometry. For HEK-Blue-NF-κB cells, the RS EVs were added directly into the wells for 48 hours and the stimulation (TNF-α, 10 ng/ml) added after another 6 hours. Luciferase signals from the cell lysate were evaluated using the GloMax® 96 Microplate Luminometer machine (Promega, USA).

Virus production

The transgenes were subcloned into our lentiviral vectors (Transfer plasmid, 22.5 µg/T175 flask) which were co-transfected with pCD/NL-BH (Helper plasmid, 22.5 µg/T175 flask) and pcoPE01 (Envelope plasmid, 3.5 µg/T175 flask) into HEK293T cells and incubated overnight. The next morning, cell medium was changed to complete DMEM medium (with 10% FBS and 1% Anti-anti) supplemented with sodium butyrate (Sigma-Aldrich). After 6 to 8 hours, the sodium butyrate containing DMEM medium was changed back to complete DMEM medium without additional chemicals. Nalgene® Oak Ridge Centrifuge Tubes (Thermo Scientific) were used for harvesting viruses 22 to 24 hours after incubation. Briefly, the virus-particle-containing medium was collected and filtered using a 0.45 µm syringe filter (VWR), and then centrifuged at 25,000 x g for 90 min at 4°C. The supernatant was aspirated, and freshly prepared medium (IMDM with 20%FBS) was used to resuspend the virus pellets. The viruses were added directly into the target cells or stored at -80°C for long-term use.

Stable reporter cell generation

HeLa, T47D, B16F10, Raw264.7, THP-1, K562, and MSC cells were seeded into 6-well plates and the viruses were added into the cells the next day. Titration of viruses was done using 3 doses: 2 µl, 10 µl, and 50 µl per well. After one day incubation of the viruses with target cells, the medium was changed back to normal complete medium (DMEM + 10% FBS + 1% Anti-anti for B16F10 and Raw264.7 cells; RPMI-1640 + 10% FBS + 1% Anti-anti for THP-1, K562, and MSC cells). Two days after virus transduction, the cells were trypsinized and resuspended in fresh medium. Resistance selection was performed by adding puromycin (2 µg/ml for B16F10 and MSC cells, 4 µg/ml for THP-1, K562, HeLa, and T47D cells, and 6 µg/ml for Raw264.7 cells). Untransduced cells died from the puromycin whereas successfully transduced cells survived and continued to grow. The cells were passaged under puromycin selection for approximately one week before the cells were utilized for downstream experiments.

Direct co-culture of EV-producing cells with reporter cells

HEK293T cells were seeded into a 6-well plate at a density of 0.5 million cells per well. The next day when the cells reached 60-70% confluence, corresponding constructs were transfected into the wells using Lipofectamine2000 (Invitrogen, USA) according to the manufacturer's protocol. Six hours after transfection, the medium was changed to fresh medium (DMEM + 10%FBS + 1% Anti-anti) to reduce the toxicity of the Lipofectamine 2000. Twenty-four hours after plasmid transfection, the cells were trypsinized, counted, and mixed with the corresponding reporter cells at ratios of 1:1 or 1:5, or other ratios as indicated in the Fig.s (ratio=EV-producing cells: reporter cells) in a 96-well plate. After co-culturing for 24 h, the cells were trypsinized and measured using the MACSQuant flow cytometer to check the percentage of GFP positive cells.

IBIDI co-culture µ-slide assay

HEK293T cells were seeded into a 6-well plate at a density of 5×10^5 cells per well. The day after, indicated constructs were transfected into cells using Lipofectamine 2000 (Invitrogen, USA) according to the manufacturer's protocol. To avoid the toxicity of the Lipofectamine2000 on the HEK293T cells, the

medium was changed to fresh complete medium (DMEM + 10%FBS + 1% Anti-anti) after 6 h. The following day, the transfected cells were trypsinized and counted. The transfected cells (feeder cells or EV-producing cells) were seeded into the surrounding reservoirs of the ibidi µ-Slide while the recipient cells (traffic-light reporter cells) were added to the central reservoir, following cell numbers indicated in the Fig.s. The volume of medium used for each reservoir was 40 µl. Once the cells were attached to the bottom, another 400 µl of complete medium (DMEM + 10%FBS + 1% Anti-anti) was added into the slide slowly and carefully to immerse the walls between the central reservoir and the surrounding reservoirs such that cell-cell communication could be mediated by engineered EVs. Four days later, the GFP positive cells were measured using either a fluorescent microscope or the MACSQuant flow cytometer.

Transwell co-culture assay

Similar to the IBIDI assay, HEK293T cells were seeded into a 6-well plate for 24 h and then transfected with the indicated constructs. The medium was changed to fresh complete medium after 6 h of transfection. One day after transfection, the cells were trypsinized and counted, and the EV-producing cells were added to the top chamber of the transwell system (pore size=0.4 µm) while the reporter cells were seeded at the bottom. After 4 days of cell-cell communication by engineered EVs, a fluorescent microscope or MACSQuant flow cytometer was used to check for GFP positive cells.

Dynamic live imaging assay

Huh7 cells were plated 1 day before the experiment in a polymer-bottom cell culture plate (Ibidi, cat. No. 82426), with 5×10^4 cells per well. 5×10^{10} EVs were added to the cells 3 hours prior imaging and Hoechst dye for nucleus staining was added just before the live cell imaging.

Confocal images were acquired on a Nikon C2 + confocal microscope equipped with an oil-immersion 60x objective with numerical aperture 1.4 (Nikon Instruments, Amsterdam, The Netherlands). The sample was excited and detected with appropriate excitation laser lines and emission filters and the fluorophores were imaged sequentially. The images were taken every hour over the course of 72 hours. The corresponding videos were generated by using the Nikon NIS-Elements Imaging Software.

Confocal microscopy

Huh7 cells were seeded in polymer-bottom cell culture plates (Ibidi, cat. no. 82426) one day before the experiment, similar to the dynamic live imaging assay. Indicated number of engineered EVs were added to the cells one day after seeding. After adding EVs for 48 hours, Hoechst dye was added before confocal microscopy imaging. The confocal images were taken the same way as described in dynamic live imaging assay. Image processing was performed by using Fiji software.

Fluorescent microscopy

After addition of EVs, co-culture, IBIDI, and Transwell assays, the GFP positive cells were visualized under a fluorescent microscope. We chose the area for taking pictures randomly and set up the same

parameters for the groups using one experiment. All the images were then processed with the same parameters in the machine or using the Fiji software.

Western blot analysis

Whole cell protein was isolated using RIPA buffer supplemented with a protease inhibitor cocktail, mixed with sample buffer (4×), and heated at 70°C for 10 min. For EV samples, 1×10^{10} EVs were mixed with sample buffer (4×) and heated at 70°C for 10 min. Samples were then loaded onto a NuPAGE™ 4-12% Bis-Tris Protein Gel (Thermo Scientific) and ran at 120 V for 2 h in NuPAGE™ MES SDS running buffer (Thermo Scientific). Proteins were transferred from the gel to the membrane using iBlot™ 2 Transfer Stacks (Thermo Scientific). The membrane was blocked with Intercept™ blocking buffer (LI-COR Biosciences) for 1 h at room temperature in a shaker after which it was incubated with primary antibodies overnight at 4°C. The membrane was washed with TBS-T buffer three times for 5 min each and incubated with corresponding secondary antibodies for 1 h at room temperature in a shaker. After washing with TBS-T buffer three times and with PBS once, the membrane was scanned using the Odyssey infrared imaging system (LI-COR).

IHC staining for melanoma tissues

Tissue sections were fixed at 65°C for 1 hour before the slides were subjected to deparaffinization and rehydration as follows: Xylene for 20 min, 100% ethanol for 3 min twice, 95% ethanol for 3 min, 70% ethanol for 3 min, and then 50% ethanol for 3 min. Afterwards, the slides were rinsed in running cold tap water for 5 min followed by antigen retrieval using citrate buffer, pH 6.0 (Sigma). After antigen retrieval, the slides were washed with PBS three times for 5 min each and immersed in blocking buffer for 30 min at 37°C. The slides were then incubated with primary anti-GFP antibody (Abcam, ab290, 1:200 dilution) overnight after blocking. The following day, after washing the slides with PBS three times for 5 min each, the slides were incubated with secondary antibody Goat Anti Rabbit IgG H&L (Alexa Fluor® 488) (Abcam, ab150077, 1:500 dilution) for 30 min at 37°C, followed by washing with PBS three times for 5 min each. The slides were mounted using ProLong™ Diamond Antifade Mountant with DAPI (Thermo Scientific) and sealed with nail polish. Images were taken using a confocal microscope (Nikon, Japan).

IHC staining for tissues from Cre-LoxP R26-LSL-tdTomato reporter mice

Tissue sections (5 μm) were made from organs of ICV and IP injected R26-LSL-tdTomato reporter mice and then were deparaffinized in xylene and ethanol, boiled in citrate buffer for 20 min, and blocked with 5% goat serum in PBS-T (PBS containing 0.3% Triton X-100) solution for 1 h at room temperature. The sections were then stained with primary antibodies in blocking buffer at 4°C overnight. After washing with PBS, sections were stained with appropriate fluorophore-conjugated secondary antibodies in PBS or PBS containing 0.1% Triton X-100 for 1 to 2 h before washing and mounting. A Zeiss LSM780 confocal microscope or Zeiss Axioscan Z.1 was used for imaging.

Statistics

Statistical tests for the biological replicates used in this study are reported in each Fig. legend. GraphPad software was utilized for the statistical analysis and the data presented as ±SD. Two-tailed T-test was used for the comparisons of two individual groups. One-way ANOVA or Two-way ANOVA multiple comparisons test was used for the analysis of the multiple groups. Log-rank (Mantel-Cox) test was used for the survival comparisons. Statistical significance was set up as * $p < 0.05$, ** $p < 0.01$; *** $p < 0.001$; **** $p < 0.0001$; ns: non-significant.

Data availability

All the data are available in the manuscript or in the supplementary information, and all the raw data from this study are available from the corresponding authors upon request. Materials are available upon signing the material transfer agreement (MTA) submitted to S.E.-A. and Evox Therapeutics Limited, Oxford, United Kingdom.

Figures

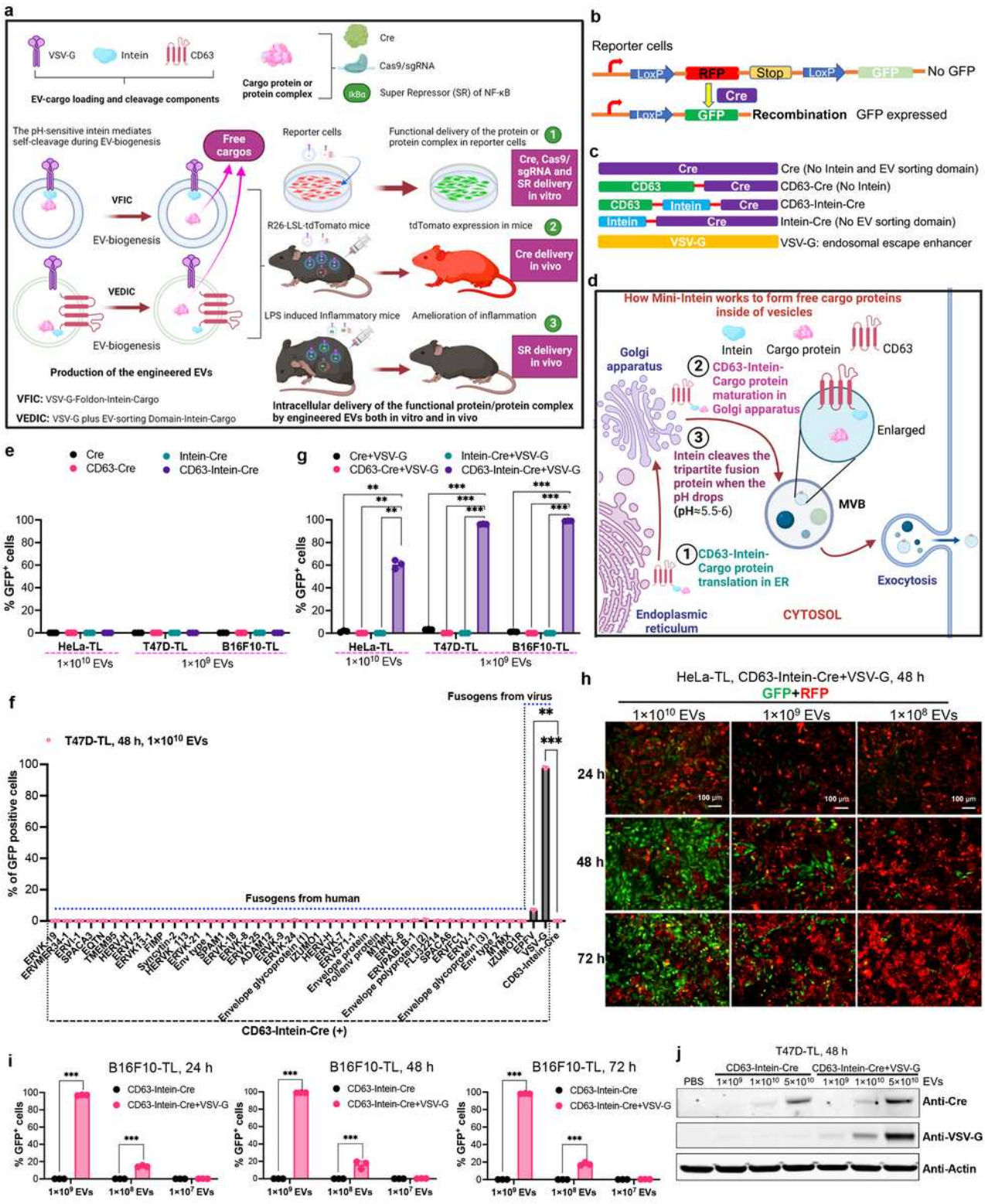

Figure 1

Development of the VEDIC system for high efficiency intracellular protein delivery by EVs. a, Graphic abstract of the development of VEDIC and VFIC systems for high efficiency intracellular protein delivery *in vitro* and *in vivo*. Intein in tripartite fusion protein (EV-sorting Domain-Intein-Cargo) performs C-terminal cleavage during the process of EV-biogenesis, resulting in enriched free cargo protein inside EVs. Together with a fusogenic protein, VSV-G, these engineered EVs achieve high-efficiency intracellular

delivery of cargo protein (Cre and super repressor of NF-κB) or protein complex (Cas9/sgRNA RNPs) both in reporter cells and in mice models. **b**, Fluorescence reporter construct expressed in the reporter cells generated to measure Cre delivery. **c**, Constructs used for developing the VEDIC system. **d,** Schematic of intein cleavage and intraluminal cargo release during EV biogenesis, MVB: multivesicular body. **e,** Percentage of GFP positive reporter cells after adding EVs for 2 days, as evaluated by flow cytometry. **f,** Fusogen screen in T47D-TL cells after a two-day incubation period with EVs. **g,**Percentage of GFP positive reporter cells after exposure to EVs derived from VSV-G co-transfected cells. **h,** EV dose-and time-dependent recombination in HeLa-TL reporter cells mediated by VEDIC EVs. **i,** EV dose-and time-dependent recombination in B16F10-TL reporter cells mediated by VEDIC EVs. **j,** Cre and VSV-G protein was detected in T47D-TL reporter cells by Western blot (WB) analysis, 48 hours (h) after addition of engineered EVs loaded with Cre in 24-well plates. Two-way ANOVA multiple comparisons test was used for analysis of (**g**) and (**i**); One-way ANOVA multiple comparisons test was used for analysis of (**f**). Data are shown as mean±SD, ** p < 0.01; *** p < 0.001.

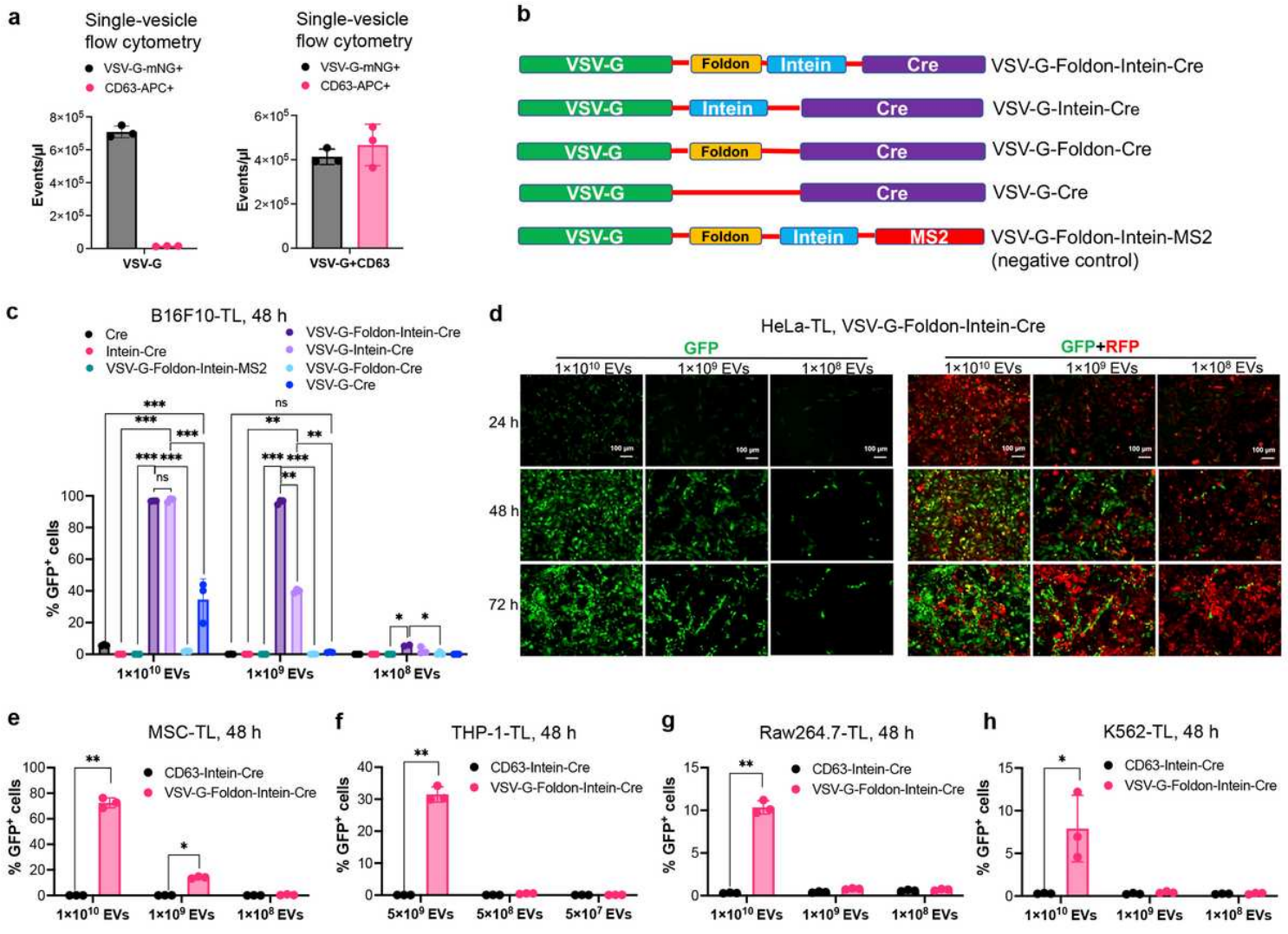

Figure 2

Development of the VFIC system to further improve intracellular protein delivery by EVs. a, VSV-G+ and CD63+ EV concentrations as determined by single-vesicle flow cytometry after transfection with VSV-G-mNG alone or VSV-G-mNG and CD63 together. **b,** Constructs generated for developing the VFIC system. The last construct was generated where Cre was replaced with the bacteriophage protein MS2, as a negative control for Cre delivery [32]. **c,** EV dose-dependent recombination in B16F10-TL cells mediated by VSV-G-Foldon-Intein-Cre and VSV-G-Intein-Cre EVs as evaluated by flow cytometry. **d,** Representative images showing GFP positive HeLa-TL cells 24, 48 and 72 h after exposure to VFIC EVs at different doses. Scale bar, 100 µm. **e-h,** Recombination in hard-to-transfect reporter cells (MSC-TL, THP-1-TL, Raw264.7-TL and K562-TL) mediated by VFIC EVs after 48 h. Two-way ANOVA multiple comparisons test was used for analysis of (**c**) and (**e-h**). Data are shown as mean±SD, * $p < 0.05$; ** $p < 0.01$; *** $p < 0.001$; ns: non-significant.

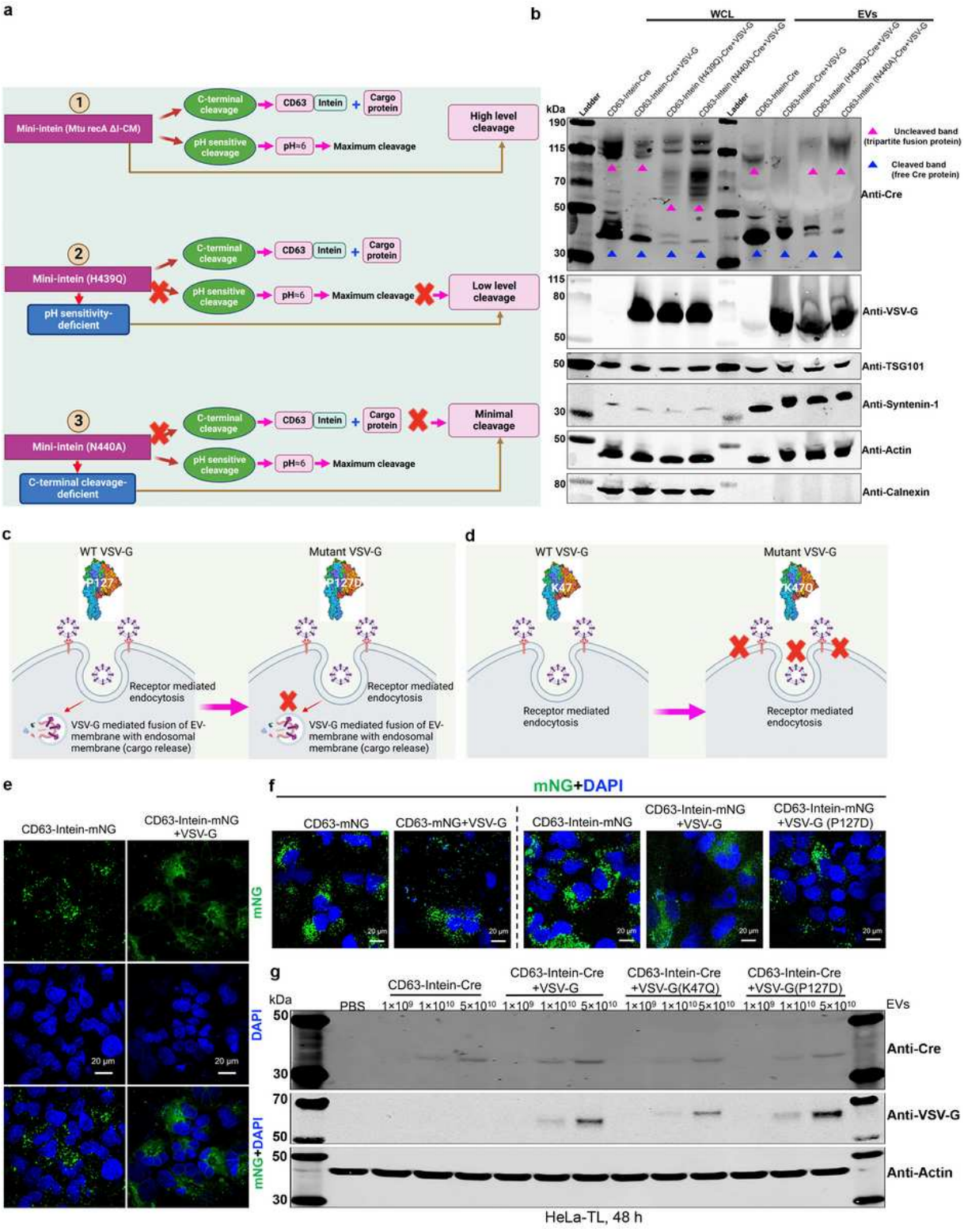

Figure 3

The underlying mechanisms responsible for intein cleavage and endosomal escape of VSV-G. **a,** Schematic illustration of the cleavage mechanism of different engineered intein variants. **b,** Protein expression of different engineered mutant intein constructs in whole cell lysates (WCL) and isolated EVs derived from HEK293T cells evaluated by WB analysis. Lysates from 5×10^5 EV-producing cells and 1×10^{10} engineered EVs were used for the assay. TSG101, syntenin-1 and β-actin were used as EV markers

and Calnexin was used as a cellular organelle marker (endoplasmic reticulum) that should be absent in EV samples. **c,d**, Properties of the two VSV-G mutants: VSV-G P127D loses the capacity to mediate fusion between the EV-and endosomal membranes and VSV-G K47Q is unable to bind to LDLR on the cell surface. **e,** Confocal immunofluorescence demonstrating the subcellular distribution of mNG in the presence or absence of wild type VSV-G engineered EVs in Huh7 cells. Scale bar, 20 μm, representative images. **f,** Subcellular distribution of mNG in different groups after adding the indicated engineered EVs determined by confocal immunofluorescence. Scale bar, 20 μm, representative images. **g,** WB evaluation of protein levels of Cre and VSV-G in HeLa-TL reporter cells after addition of engineered EVs with wild type, P127D or K47Q VSV-G in 24-well plates.

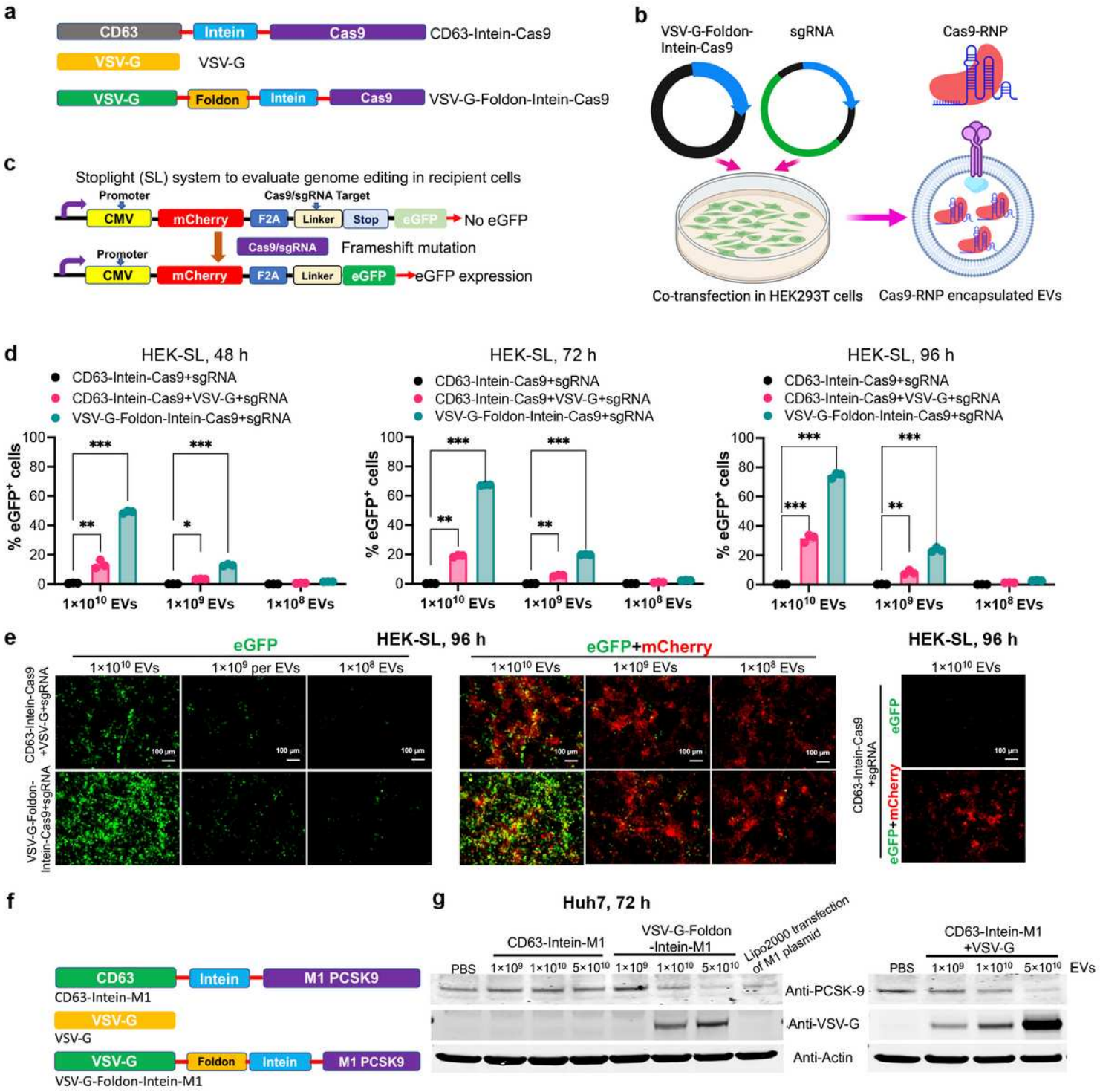

Figure 4

Robust gene editing by Cas9/sgRNA RNP and meganuclease targeting PCSK9 using the VFIC and VEDIC systems. a, Constructs generated for Cas9/sgRNA RNPs delivery. **b,** Schematic illustration about how the Cas9/sgRNA RNPs were encapsulated into engineered EVs. **c,** Schematic of reporter cells used to functionally assess Cas9/sgRNA RNPs delivery by engineered EVs. **d,**Percentage of eGFP positive cells after addition of engineered EVs, as measured by flow cytometry 48, 72 and 96 h after EV addition. **e,** Immunofluorescence demonstrated gene-editing in recipient cells after treatment with different doses of

engineered EVs after 4 days. Scale bar, 100 μm, representative images. **f,** Constructs generated for EV-mediated delivery of meganuclease targeting PCSK9. **g,** WB analysis of PCSK9 and VSV-G protein in Huh7 cells after treatment with different doses of EVs in 24-well plates. Two-way ANOVA multiple comparisons test was used for analysis of (**d**). Data are shown as mean±SD, * $p < 0.05$; ** $p < 0.01$; *** $p < 0.001$.

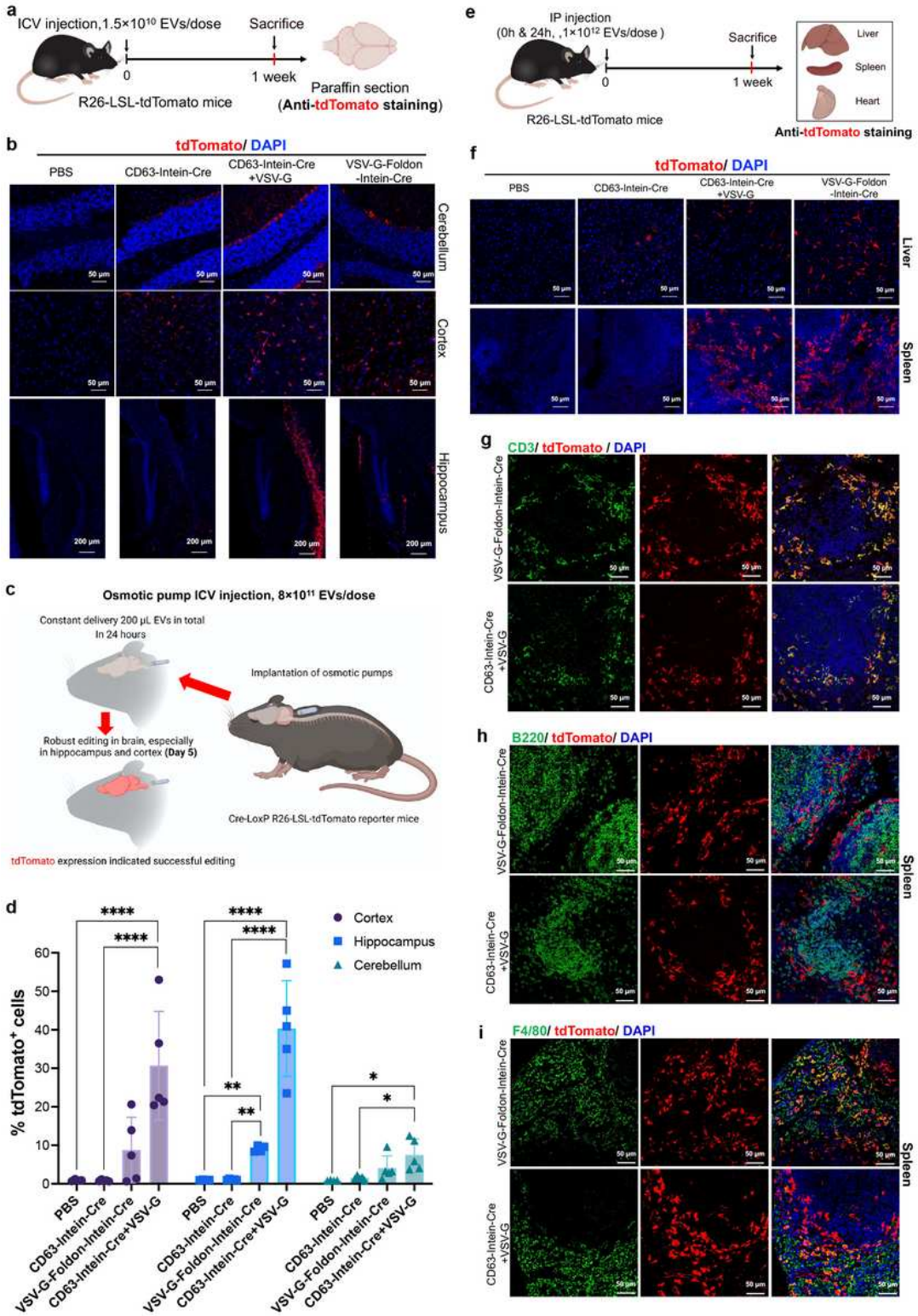

Figure 5

Cre recombination in R26-LSL-tdTomato reporter mice by VEDIC and VFIC engineered EVs after local (ICV or osmotic pump ICV) and systemic (IP) injections. a,Workflow for the intracerebroventricular (ICV) injection of engineered EVs to deliver Cre in the brains of R26-LSL-tdTomato reporter mice. **b,** TdTomato expression in different regions of brain after ICV injection of engineered EVs, as determined by immunofluorescence. Scale bar, 50 μm for cerebellum and cortex, and 200 μm for hippocampus. **c,** Workflow for the osmotic pump ICV injection of engineered EVs to transfer Cre to the brain tissues of R26-LSL-tdTomato reporter mice. **d,** Percentage of tdTomato+ cells in the brain tissues after osmotic pump ICV injection of engineered EVs for 5 days. n=4 mice for PBS group whereas n=5 mice for other groups. **e,** Schematic workflow for the intraperitoneal (IP) injection of engineered EVs into R26-LSL-tdTomato reporter mice. **f,** TdTomato expression in liver and spleen after IP injection of engineered EVs for one week. Scale bar, 50 μm. **g,** Co-staining of tdTomato with the T cell marker CD3 in spleen as detected by immunofluorescence one week after IP injection of engineered EVs. Scale bar, 50 μm. **h,** Co-staining of tdTomato with the B cell marker B220 in spleen one week after IP injection of engineered EVs. Scale bar, 50 μm.

i, Co-staining of tdTomato and the macrophage marker F4/80 in spleen one week after IP injection of engineered EVs. Scale bar, 50 μm. n=3 mice per group, representative images for (**b**) and (**f**-**i**). Two-way ANOVA multiple comparisons test was used for analysis of (**d**). Data are shown as mean±SD, * $p < 0.05$; ** $p < 0.01$; **** $p < 0.0001$.

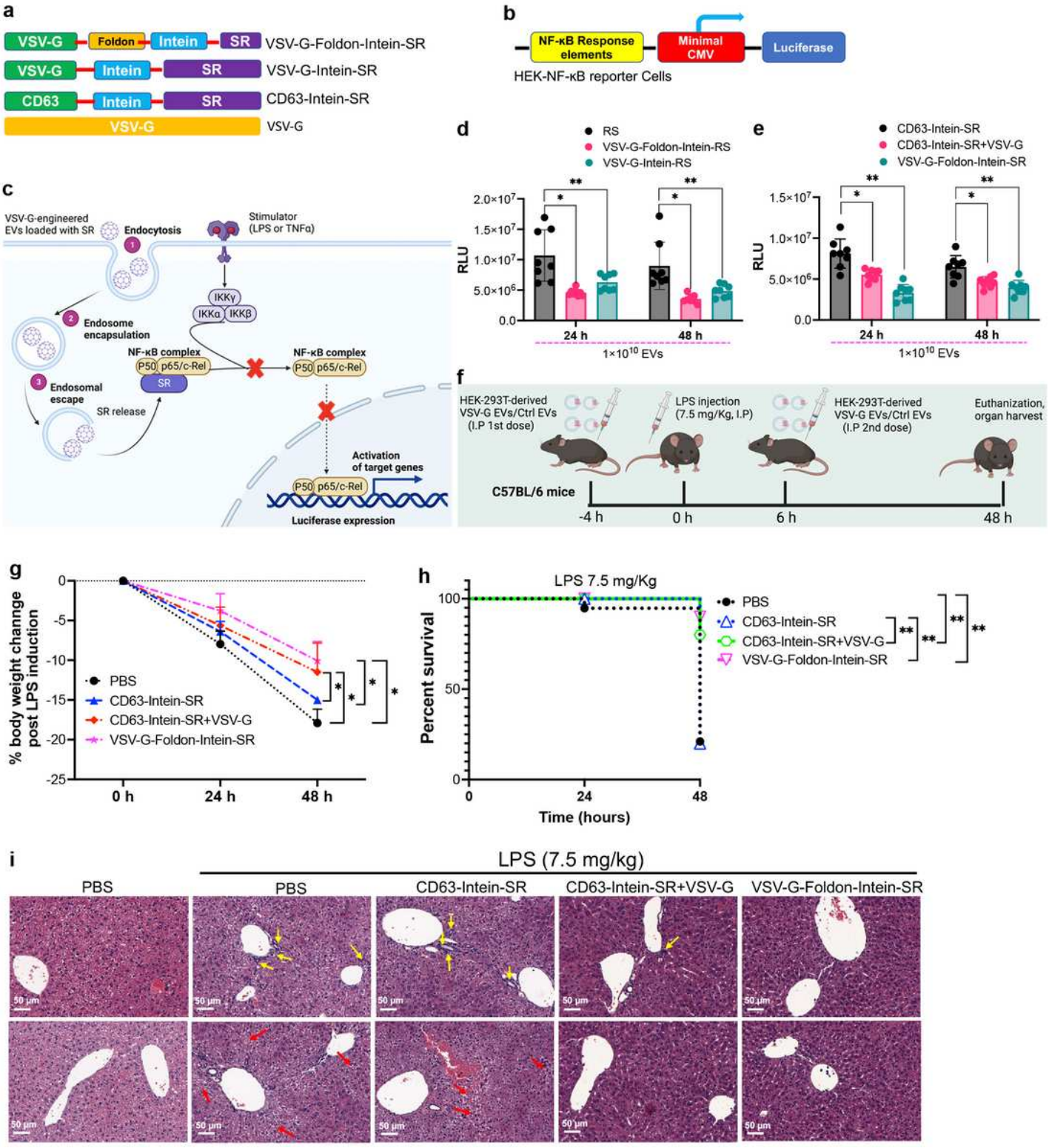

Figure 6

Treatment of LPS-induced systemic inflammation using VEDIC and VFIC-EV mediated delivery of a super-repressor of NF-κB. a, **b**, Design of the constructs and reporter cells utilized for delivery and assessment of a super-repressor of NF-κB by engineered EVs. **c,** Schematic illustration how the EV-delivered super-repressor of NF-κB inhibits NF-κB activity. **d,e**, Luciferase activity from HEK-NF-κB reporter cells, 24 or 48 h after treatment with engineered EVs respectively (TNF-α stimulation for 6 h before harvesting cells), in

24-well plates. **f,** Schematic illustration of the workflow for the treatment of LPS-induced systemic inflammation by engineered EVs in mice (5×10^{11} EVs/mouse per dose). **g,h**, Percentage of body weight loss and group survival in mice after LPS and engineered EV injections. n=10 mice per group. **i,** Representative histology images (hematoxylin-eosin stain) of liver to show the aggregation of inflammatory cells (upper panel, yellow arrows indicate the aggregated inflammatory cells in portal areas) and the hydropic degeneration of hepatocytes (lower panel, red arrows indicate the hydropic degeneration of hepatocytes) after LPS induction. Scale bar, 50 μm. Two-way ANOVA multiple comparisons test was used for analysis of (**d, e,** and **g**); Log-rank (Mantel-Cox) test was used for the analysis of survival curve (**h**). Data are shown as mean±SD for (**d, e,** and **g**). * $p < 0.05$; ** $p < 0.01$.

Supplementary Files

This is a list of supplementary files associated with this preprint. Click to download.

- SupplementaryInformation.docx
- SupplementaryVideo1.VEDICEVgroup..mov
- SupplementaryVideo2.ControlEVgroup..mov
- SupplementaryVideo3.VFICEVgroup..mov